Three-dimensional analysis of harmonic generation in high-gain free-electron lasers

Zhirong Huang and Kwang-Je Kim
Advanced Photon Source, Argonne National Laboratory, Argonne, Illinois 60439
(Received 8 May 2000)

In a high-gain free-electron laser (FEL) employing a planar undulator, strong bunching at the fundamental wavelength can drive substantial bunching and power levels at the harmonic frequencies. In this paper we investigate the three-dimensional evolution of harmonic radiation based on the coupled Maxwell-Klimontovich equations that take into account nonlinear harmonic interactions. Each harmonic field is a sum of a linear amplification term and a term driven by nonlinear harmonic interactions. After a certain stage of exponential growth, the dominant nonlinear term is determined by interactions of the lower nonlinear harmonics and the fundamental radiation. As a result, the gain length, transverse profile, and temporal structure of the first few harmonics are eventually governed by those of the fundamental. Transversely coherent third-harmonic radiation power is found to approach 1% of the fundamental power level for current high-gain FEL projects.

PACS number(s): 41.60.Cr, 42.55.Vc, 42.65.Ky

I. INTRODUCTION

The ability to generate coherent harmonic radiation is an important aspect of a free-electron laser (FEL). In a planar undulator with a strong magnetic field, spontaneous emissions at the fundamental resonant frequency and its higher harmonics induce bunching at their respective wavelength scales, leading to amplified emissions [1], but the linear amplification of the higher harmonics is always smaller than the fundamental. For a fourth-generation light source based on a single-pass, high-gain FEL amplifier, the fundamental is always heavily favored because of its advantage in gain length. Even for a subharmonically seeded high-gain harmonic generation (HGHG) FEL scheme [2] that employs two undulators with the second undulator resonant to one of the harmonics of the first and a dispersion section between them, the lasing still occurs at the fundamental of the second undulator.

Nevertheless, coherent harmonic emission is generated when the laser fundamental bunches the electron beam strongly, producing Fourier components at the harmonics. For a high-gain FEL, a one-dimensional (1D) model [3] and a three-dimensional simulation study [4] indicate that significant powers of the first few harmonics are generated through nonlinear harmonic interactions. In this paper, we present a 3D analysis of harmonic generation in a high-gain FEL based on the coupled Maxwell-Klimontovich equations. Starting from the fundamental, we determine the dominant contributions to the first few harmonics and their radiation characteristics such as gain length, transverse profile, and temporal structure in a high-gain FEL. Since the nonlinear harmonic generation occurs naturally in one long planar undulator, it exists both for a self-amplified spontaneous emission (SASE) FEL with an initially uniform bunch and for the second stage of an HGHG FEL using a density-modulated bunch. Thus, such a harmonic generation mechanism may be utilized to reach shorter radiation wavelengths or to relax some stringent requirements on the electron-beam quality for a fourth-generation light source. Explicit calculations based on current high-gain FEL projects show that the power of the transversely coherent third-harmonic radiation can approach 1% of the fundamental power level.

This paper is organized as follows. In Sec. II, the coupled Maxwell-Klimontovich equations are employed for the self-consistent treatment of the beam-radiation interaction. Scaled variables and parameters are introduced to simplify the notation. In Sec. III, we extend the 3D analysis of the linear interaction from the fundamental frequency to its higher harmonics and show that the linear amplification process occurs predominantly around the fundamental frequency. The matrix formulation of Xie [5] is used in solving the dispersion relation to determine the transverse guided mode that has the largest growth rate. In Sec. IV, we include nonlinear harmonic interactions into our perturbation analysis and demonstrate that the nonlinear harmonic generation is primarily driven by the radiation field at the fundamental frequency and can be much stronger than the linear harmonic generation. Generation of the third-harmonic radiation due to this nonlinear mechanism is studied for both coherent amplification and self-amplified spontaneous emission in Sec. V. Numerical examples drawn from current high-gain FEL projects are used in Sec. VI to show that significant third-harmonic power can develop before FEL saturation. A summary of these results and some concluding remarks are given in the concluding section.

II. COUPLED MAXWELL-KLIMONTOVICH EQUATIONS

Consider a planar undulator with a sinusoidal magnetic field in the y direction. For an electron beam with average energy $\gamma_0 mc^2$, the transverse wiggling motion is accompanied by a longitudinal oscillation around the average longitudinal position at twice the transverse frequency ck_u (a figure-eight motion in the electron's co-moving frame). Such a nonsinusoidal trajectory can give rise to harmonic radiation. Let us represent the electric field in the form

$$\hat{x}\int_{-\infty}^{\infty}\frac{d\nu}{2}E(\nu,\boldsymbol{x},z)e^{i\nu k_1(z-ct)}, \tag{1}$$

where $\boldsymbol{x}=(x,y)$ represents the transverse coordinates, $ck_1=(2\gamma_0^2 ck_u)/(1+K^2/2)$ is the fundamental resonant frequency, $k_u=2\pi/\lambda_u$, λ_u is the undulator period length, K is

the undulator parameter, and $|E(\nu)|$ is the field amplitude at frequency $\nu k_1 c$ providing that $E(-\nu)=E^*(\nu)$. If E is assumed to vary slowly with z, the Maxwell equation under the paraxial approximation becomes

$$\int_{-\infty}^{\infty}\frac{d\nu}{2}e^{i\nu k_1(z-ct)}\left(2i\nu k_1\frac{\partial}{\partial z}+\nabla_\perp^2\right)E(\nu,\mathbf{x},z)$$
$$=\frac{1}{\epsilon_0 c^2}\frac{\partial}{\partial t}J_x(\mathbf{x},z,t), \tag{2}$$

where $\nabla_\perp^2$ is the transverse Laplacian, ϵ_0 is the permittivity of free space, and the transverse current density for a beam of N_e electrons is given by

$$J_x=ecK\cos(k_u z)\sum_{j=1}^{N_e}\frac{1}{\gamma_j}\delta[\mathbf{x}-\mathbf{x}_j(t)]\delta[z-z_j(t)], \tag{3}$$

where $\gamma_j mc^2$ and $(\mathbf{x}_j,z_j)$ are the energy and the position of the jth electron. Inverting Eq. (2) yields

$$\left(\frac{\partial}{\partial z}+\frac{\nabla_\perp^2}{2i\nu k_1}\right)E(\nu,\mathbf{x},z)$$
$$=\frac{1}{\epsilon_0 c^2}\int_{-\infty}^{\infty}\frac{c\,dt}{2i\nu\pi}e^{-i\nu k_1(z-ct)}\frac{\partial}{\partial t}J_x(\mathbf{x},z,t)$$
$$\approx-\frac{eK}{\epsilon_0\gamma_0}\int_{-\infty}^{\infty}\frac{ck_1 dt}{2\pi}e^{-i\nu k_1(z-ct)}\cos(k_u z)$$
$$\times\sum_{j=1}^{N}\delta[\mathbf{x}-\mathbf{x}_j(t)]\delta[z-z_j(t)]. \tag{4}$$

Here we have approximated $\gamma_j=\gamma_0$ in the transverse velocity of the beam (assuming the energy spread is small) and performed integration by parts over the time variable.

It is convenient to treat z, the distance from the undulator entrance, as the independent variable, and change the dependent coordinate from t to θ by $\theta(z)=(k_u+k_1)z-ck_1t^*=(k_u+k_1)z-ck_1t+\xi\sin(2k_u z)$, where ct^* denotes the average electron position and $\xi=K^2/(4+2K^2)$. The right-hand side of Eq. (4) becomes

$$-\frac{eK}{\epsilon_0\gamma_0}\int_{-\infty}^{\infty}\frac{k_1 d\theta}{2\pi}e^{-i\nu\theta}\exp i\nu k_u z+i\nu\xi\sin(2k_u z)$$
$$\times\cos(k_u z)\sum_{j=1}^{N_e}\delta[\mathbf{x}-\mathbf{x}_j(z)]\delta[\theta-\theta_j(z)], \tag{5}$$

where $\theta_j(z)$ describes the FEL bunching action, and $\mathbf{x}_j(z)$ contains both the transverse wiggling motion (in the x plane) and the betatron oscillation. Since the FEL interaction and the betatron oscillation occur on a scale much longer than the fast wiggling motion, we average Eq. (5) over the undulator period λ_u with the help of the Bessel function expansion

$$e^{i\nu\xi\sin(2k_u z)}=\sum_{p=-\infty}^{+\infty}J_p(\nu\xi)e^{i2pk_u z}. \tag{6}$$

Furthermore, because the transverse wiggling amplitude is normally smaller than the transverse dimension of the electron beam, we neglect the wiggling motion in the transverse current distribution function $\delta[\mathbf{x}-\mathbf{x}_j(z)]$ when taking the wiggling average. Hence, the wiggling averaged Eq. (5) is nonzero only when ν is close to an odd integer $h=-(2p\pm1)=\cdots-5,-3,-1,1,3,5,\ldots$, and we obtain for the field amplitude $E(h+\Delta\nu_h,\mathbf{x},z)$ near the hth harmonic

$$\left(\frac{\partial}{\partial z}+\frac{\nabla_\perp^2}{2ihk_1}\right)E(h+\Delta\nu_h,\mathbf{x},z)$$
$$=-\frac{eK_h}{2\epsilon_0\gamma_0}e^{i\Delta\nu_h k_u z}\int\frac{k_1 d\theta}{2\pi}e^{-i\nu\theta}$$
$$\times\sum_{j=1}^{N_e}\delta(\mathbf{x}-\mathbf{x}_j)\delta(\theta-\theta_j). \tag{7}$$

Here we have defined the effective coupling strength of the hth harmonic as

$$K_h=K(-1)^{(h-1)/2}[J_{(h-1)/2}(h\xi)-J_{(h+1)/2}(h\xi)]. \tag{8}$$

In the forward z direction, the electric field consists of a series of nearly monochromatic waves around the odd harmonic frequencies hck_1 [1], with the frequency detuning $\Delta\nu_h=\nu-h\ll1$. Retaining the wiggling motion in the transverse current distribution function $\delta[\mathbf{x}-\mathbf{x}_j(z)]$ would lead to even harmonic emissions [6], which normally have lower power levels than their odd counterparts for a high-gain FEL [4]. The generation of even harmonics will be neglected in this paper and will be discussed in a future publication [7].

The microscopic electron distribution in the phase space is given by the Klimontovich distribution function [8]:

$$F(z,\theta,\eta,\mathbf{x},\mathbf{p})=\frac{k_1}{n_0}\sum_{j=1}^{N_e}\delta(\theta-\theta_j)\delta(\eta-\eta_j)\delta(\mathbf{x}-\mathbf{x}_j)$$
$$\times\delta(\mathbf{p}-\mathbf{p}_j), \tag{9}$$

where $\eta=(\gamma-\gamma_0)/\gamma_0$ and $\mathbf{p}=d\mathbf{x}/dz$ are the energy and transverse momentum variables, respectively, and n_0 is the peak electron volume density. Equation (7) becomes

$$\left(\frac{\partial}{\partial z}+\frac{\nabla_\perp^2}{2ihk_1}\right)E(h+\Delta\nu_h,\mathbf{x},z)$$
$$=-\kappa_h n_0 e^{i\Delta\nu_h k_u z}\int\frac{d\theta}{2\pi}e^{-i\nu\theta}\int d^2p\int d\eta F, \tag{10}$$

where $\kappa_h=eK_h/(2\epsilon_0\gamma_0)$.

The evolution of the Klimontovich distribution function F is governed by the continuity equation

$$\frac{\partial F}{\partial z}+\dot\theta\frac{\partial F}{\partial\theta}+\dot\eta\frac{\partial F}{\partial\eta}+\dot{\mathbf{x}}\frac{\partial F}{\partial\mathbf{x}}+\dot{\mathbf{p}}\frac{\partial F}{\partial\mathbf{p}}=0. \tag{11}$$

Here the dot means d/dz and the equations of motion are

$$\dot\eta=\sum_h\kappa_h'\int d(\Delta\nu_h)e^{i\nu\theta}e^{-i\Delta\nu_h k_u z}E(h+\Delta\nu_h,\mathbf{x},z), \tag{12}$$

$$\dot\theta=2k_u\eta-\frac{k_1}{2}(\mathbf{p}^2+k_\beta^2\mathbf{x}^2), \tag{13}$$

$$\dot{\boldsymbol{p}}=-k_\beta^2\boldsymbol{x}, \quad \text{and} \quad \dot{\boldsymbol{x}}=\boldsymbol{p}, \tag{14}$$

where $\kappa_h'=eK_h/4\gamma_0^2mc^2$, and k_β is the effective total (natural and external) focusing strength in both transverse planes. The energy equation (12) and the phase equation (13) generalize Colson's pendulum equations [1] to the 3D case, and the transverse betatron motion is described by Eq. (14) under the smooth approximation. When only natural undulator focusing is present, $k_\beta=Kk_u/(2\gamma_0)$, and $(\boldsymbol{p}^2+k_\beta^2\boldsymbol{x}^2)$ is a constant of motion in the phase equation (13), as noted by Scharlemann [9]. However, in many high-gain FELs, external focusing much stronger than the natural one is required to reduce the gain length. In this case, it can be shown [10] that the same factor $(\boldsymbol{p}^2+k_\beta^2\boldsymbol{x}^2)$ enters the phase equation (13) and is also a constant of motion.

Using the method of integration along the unperturbed trajectory [11], the continuity equation can be written as the integral equation

$$\begin{aligned}F(z,\theta,\eta,\boldsymbol{x},\boldsymbol{p})=F_0-\int_0^z ds\sum_h \kappa_h'\int d(\Delta\nu_h)e^{i\nu\theta^{(0)}}e^{-i\Delta\nu_h k_w s}\\ \times E(h+\Delta\nu_h,\boldsymbol{x}^{(0)},s)\\ \times\frac{\partial}{\partial\eta}F(s,\theta^{(0)},\eta,\boldsymbol{x}^{(0)},\boldsymbol{p}^{(0)}),\end{aligned} \tag{15}$$

where F_0 is the initial electron distribution that includes the smooth distribution, the shot noise, and any initial density modulation, and the unperturbed trajectory is described by

$$\theta^{(0)}=\theta+\dot{\theta}(s-z)=\theta+\left[2k_u\eta-\frac{k_1}{2}(p^2+k_\beta^2r^2)\right](s-z),$$

$$\boldsymbol{x}^{(0)}=\boldsymbol{x}\cos[k_\beta(s-z)]+\frac{\boldsymbol{p}}{k_\beta}\sin[k_\beta(s-z)],$$

$$\boldsymbol{p}^{(0)}=-k_\beta\boldsymbol{x}\sin[k_\beta(s-z)]+\boldsymbol{p}\cos[k_\beta(s-z)]. \tag{16}$$

One important quantity of the system is the Pierce parameter ρ [12], defined through the relation $\kappa_1 n_0\kappa_1'=4k_u^2\rho^3$. It is then convenient to introduce the following scaled variables

$$\bar{z}=2\rho k_u z, \quad \bar{\eta}=\frac{\eta}{\rho}, \quad \bar{\nu}=\frac{\Delta\nu}{2\rho},$$

$$\bar{\boldsymbol{x}}=\boldsymbol{x}\sqrt{2k_1k_u\rho}, \quad \bar{\boldsymbol{p}}=\boldsymbol{p}\sqrt{\frac{k_1}{2k_u\rho}}, \tag{17}$$

as well as the scaled radiation field a_h and the scaled distribution function f:

$$a_h=\frac{-eK_h}{4\gamma_0^2mc^2k_u\rho}e^{-i\Delta\nu_h k_u z}E(h+\Delta\nu_h,\boldsymbol{x},z), \quad f=\frac{2k_u\rho^2}{k_1}F. \tag{18}$$

Equations (10) and (15) can be scaled accordingly:

$$\left(\frac{\partial}{\partial\bar{z}}+i\bar{\nu}_h+\frac{\bar{\nabla}_\perp^2}{2ih}\right)a_h=\left(\frac{K_h}{K_1}\right)^2\int\frac{2\rho d\theta}{2\pi}e^{-i\nu\theta}\int d^2\bar{p}\int d\bar{\eta}f(\bar{z},\theta,\bar{\eta},\bar{\boldsymbol{x}},\bar{\boldsymbol{p}}), \tag{19}$$

$$f=f_0+\int_0^{\bar{z}}d\bar{s}\sum_h\int d(\bar{\nu}_h)e^{i\nu\theta^{(0)}}a_h(\bar{\nu}_h,\bar{\boldsymbol{x}}^{(0)},\bar{s})\times\frac{\partial}{\partial\bar{\eta}}f(\bar{s},\theta^{(0)},\bar{\eta},\bar{\boldsymbol{x}}^{(0)},\bar{\boldsymbol{p}}^{(0)}). \tag{20}$$

Here $\theta^{(0)}=\theta+\phi(\bar{s}-\bar{z})$ is the unperturbed phase,

$$\phi=\bar{\eta}-\frac{\bar{\boldsymbol{p}}^2+\bar{k}_\beta^2\bar{\boldsymbol{x}}^2}{2} \tag{21}$$

describes the inhomogeneous effects of the energy spread and the emittance, and $\bar{k}_\beta=k_\beta/(2k_u\rho)$ is the scaled focusing strength.

III. LINEAR HARMONIC GENERATION

The coupled Maxwell-Klimontovich Eqs. (19) and (20) can be solved in perturbation theory. First, one notices that

$$\tilde{a}_h(\theta,\bar{\mathbf{x}},\bar{z})=\int d\bar{\nu}_h a_h(\bar{\nu}_h,\bar{\mathbf{x}},\bar{z})e^{i\bar{\nu}_h 2\rho\theta} \tag{22}$$

is the slowly varying radiation field along the bunch position θ. The radiation intensity I_1 at the fundamental is expected to reach saturation when [12]

$$\frac{I_1}{\rho I_{\text{beam}}}=|\tilde{a}_1(\theta)|^2\leqslant 1, \tag{23}$$

where $I_{\text{beam}}=\gamma_0mc^3n_0$ is the peak electron beam intensity. In the small signal regime before saturation, the field amplitudes $|\tilde{a}_h|\leqslant|\tilde{a}_1|<1$. To the first order in the field amplitudes, we can replace f at the right-hand side of Eq. (20) by the smooth background distribution $\bar{f}_0$ to obtain

$$f=\bar{f}_0+\hat{f}_0+\int_0^{\bar{z}}d\bar{s}\sum_h\int d(\bar{\nu}_h)e^{i\nu\theta^{(0)}}a_h(\bar{\nu}_h,\bar{\mathbf{x}}^{(0)},\bar{s})\times\frac{\partial}{\partial\bar{\eta}}\bar{f}_0(\bar{s},\theta^{(0)},\bar{\eta},\bar{\mathbf{x}}^{(0)},\bar{\mathbf{p}}^{(0)}), \tag{24}$$

where $\hat{f}_0$ contains the shot noise and any initial density modulation (as in a HGHG FEL), and is treated as a first-order quantity.

We now assume that the initial electron beam is matched to the undulator channel and is uniform in θ (this can be approximately satisfied by a bunch that is very long compared to the fundamental radiation wavelength). Taking $\bar{f}_0=\bar{f}_0(\bar{\boldsymbol{p}}^2+\bar{k}_\beta^2\bar{\boldsymbol{x}}^2,\bar{\eta})$ in Eq. (24) and inserting it into Eq. (19), we find that the field at each frequency amplifies itself

through the linear interaction and does not interact with other Fourier components. The linear harmonic generation is governed by

$$\left(\frac{\partial}{\partial\bar{z}}+i\bar{\nu}_h+\frac{\bar{\nabla}_\perp^2}{2ih}\right)a_h^L(\bar{\nu}_h,\bar{\mathbf{x}},\bar{z})-\left(\frac{K_h}{K_1}\right)^2 \times\int d^2\bar{p}\int d\bar{\eta}\int_0^{\bar{z}}d\bar{s}e^{ih\phi(\bar{s}-\bar{z})}a_h^L(\bar{\nu}_h,\bar{\mathbf{x}}^{(0)},\bar{s})\frac{\partial\bar{f}_0}{\partial\bar{\eta}} =\left(\frac{K_h}{K_1}\right)^2\int d^2\bar{p}\int d\bar{\eta}\hat{f}_{0,h}(\bar{\nu}_h,\bar{\mathbf{x}},\bar{\mathbf{p}},\bar{\eta}), \tag{25}$$

where $\hat{f}_{0,h}(\bar{\nu}_h)$ is the Fourier component of $\hat{f}_0$ at frequency detuning $\bar{\nu}_h$ near the hth harmonic. We seek a solution of the form $e^{-i\mu_h\bar{z}}A_h^L(\bar{\mathbf{x}})$, where the complex growth rate μ_h and the transverse mode profile $A_h^L(\bar{\mathbf{x}})$ satisfy the dispersion relation (as shown in Appendix A)

$$\left(-i\mu_h+i\bar{\nu}_h+\frac{\bar{\nabla}_\perp^2}{2ih}\right)A_h^L(\bar{\mathbf{x}})-\left(\frac{K_h}{K_1}\right)^2 \times\int d^2\bar{p}\int d\bar{\eta}\int_{-\infty}^0 d\tau A_h^L(\bar{\mathbf{x}}^{(0)})e^{i(h\phi-\mu_h)\tau}\frac{\partial\bar{f}_0}{\partial\bar{\eta}}=0. \tag{26}$$

Here $\bar{\mathbf{x}}^{(0)}=\bar{\mathbf{x}}\cos(\bar{k}_\beta\tau)+(\bar{\mathbf{p}}/k_\beta)\sin(\bar{k}_\beta\tau)$. This result generalizes the dispersion relation for the fundamental frequency ($h=1$) [13,14] to arbitrary harmonics. The 1D, ideal beam limit of Eq. (26) (where all transverse modes degenerate) was studied in Ref. [15]. The complex growth rate μ_h can be obtained by variational approximations [14,5] or by a matrix formulation of Eq. (26) [5]. Among all the transverse modes, the one with the largest imaginary part of μ_h is the most dominant due to exponential growth and is regarded as the guided mode. Using Van Kampen's normal-mode expansion illustrated in Appendix A, Eq. (25) can be solved for any given initial condition. In the high-gain limit, we may keep only the dominant mode and arrive at

$$a_h^L(\bar{\nu}_h,\bar{\mathbf{x}},\bar{z})\propto e^{-i\mu_h\bar{z}}A_h^L(\bar{\mathbf{x}})\Bigg[\int d^2\bar{x}'A_h^L(\bar{\mathbf{x}}')a_{0,h}(\bar{\nu}_h,\bar{\mathbf{x}}') +\int d^2\bar{x}'\int d^2\bar{p}\int d\bar{\eta}\hat{f}_{0,h}(\bar{\nu}_h,\bar{\mathbf{x}}',\bar{\mathbf{p}},\bar{\eta}) \times\int_{-\infty}^0 d\tau A_h^L(\bar{\mathbf{x}}^{(0)})e^{i(h\phi-\mu_h)\tau}\Bigg]. \tag{27}$$

The first term in the squared bracket describes the process of coherent amplification (CA) [12], which starts from a coherent input signal $a_{0,h}$ with a well-defined frequency detuning $\bar{\nu}_h$. The second term describes the process of SASE [16,13], which starts from white noise.

In this paper, we adopt the matrix formulation for the study of both linear and nonlinear harmonic interactions. Following the derivation of Ref. [5], we introduce the Hankel transform pair for the guided mode of the hth harmonic field

$$A_h(Q)=\int_0^\infty RdRJ_0(QR)A_h(R),$$

$$A_h(R)=\int_0^\infty QdQJ_0(QR)A_h(Q), \tag{28}$$

where $R=r_{\sigma_x}$, and $r=\sqrt{x^2+y^2}$. Equation (26) can be converted to an integral equation [5]

$$A_h^L(Q)=\int_0^\infty Q'dQ'T_h(Q,Q')A_h^L(Q'), \tag{29}$$

with the kernel

$$T_h(Q,Q')=\frac{h}{(\mu_h-\bar{\nu}_h)-Q^2/(2h\bar{\sigma}_x^2)}\left(\frac{K_h}{K_1}\right)^2 \times\int_{-\infty}^0\frac{\tau d\tau}{(1+ih\bar{k}_\beta^2\bar{\sigma}_x^2\tau)^2}J_0\left(\frac{iQQ'\cos\bar{k}_\beta\tau}{1+ih\bar{k}_\beta^2\bar{\sigma}_x^2\tau}\right) \times\exp\left[-\frac{h^2\bar{\sigma}_\eta^2\tau^2}{2}-i\mu_h\tau-\frac{(Q^2+Q^{*2})}{2(1+ih\bar{k}_\beta^2\bar{\sigma}_x^2\tau)}\right]. \tag{30}$$

Here the initial electron-beam distribution is assumed to be Gaussian in $(\bar{\mathbf{x}},\bar{\mathbf{p}},\bar{\eta})$, with $\bar{\sigma}_x=\sigma_x\sqrt{2k_1k_u\rho}$ and $\bar{\sigma}_\eta=\sigma_\eta/\rho$ as the scaled rms transverse size and the scaled rms energy spread, respectively. The electron-beam emittance is given by $\epsilon=\bar{\sigma}_x^2\bar{k}_\beta/k_1$. Note that we use slightly different scaling parameters from Ref. [5]. By discretizing Q and Q' to $Q_1,Q_2,\ldots,Q_N$, Eq. (29) can be cast into a matrix form

$$[\mathbf{I}-\mathbf{T}_h(\mu_h)]\mathbf{A}_h^L=0, \tag{31}$$

where $\mathbf{I}$ is the identity matrix, the matrix element $T_h^{nn'}=Q_{n'}(Q_{n'}-Q_{n'-1})T_h(Q_n,Q_{n'})$ (n and $n'=1,2,\ldots,N$, $Q_0=0$), and the vector $\mathbf{A}_h^L$ represents the eigenmode $A_h^L(Q)$ at $Q=Q_1,Q_2,\ldots,Q_N$. For a given detuning $\bar{\nu}_h$, the eigenvalue of the matrix $(\mathbf{I}-\mathbf{T}_h)$ that has the largest $\mathrm{Im}(\mu_h)$ yields the growth rate of the guided mode for each harmonic, and the Hankel transform of the corresponding eigenmode yields the transverse profile of the guided mode.

In general, the growth rate of the hth ($h>1$) harmonic is much smaller than that of the fundamental frequency because the harmonic radiation has lower coupling coefficient [i.e., $(K_h/K_1)^2<1$] and is more sensitive to the warm-beam effects (energy spread and emittance) due to the h factor in the exponent of Eq. (26), especially for the x-ray FEL's (see numerical examples in Sec. VI). Hence the linear gain process is predominantly the growth of radiation around the fundamental frequency in the exponential growth regime.

IV. NONLINEAR HARMONIC INTERACTIONS

When a beam is strongly bunched in the ponderomotive potential formed by the undulator field and the radiation field of the fundamental frequency, the bunch spectrum develops rich harmonic contents. Coherent radiation at the odd har-

monics can be generated in a planar undulator and significant power levels for the first few harmonics can be reached before the FEL saturates [3,4]. Here we study this process in detail.

To include nonlinear harmonic interactions, we iterate Eq. (20) to an arbitrary order in $\Sigma_h \int d\bar{\nu}_h e^{i\nu\theta} a_h = \Sigma_h e^{ih\theta} \tilde{a}_h$:

$$f = \bar{f}_0 + f^{(1)} + f^{(2)} + \cdots + f^{(m)} + \cdots, \tag{32}$$

where the first-order distribution is given in Eq. (24) and the mth order ($m>1$) distribution function is

$$\begin{aligned} f^{(m)} = & \int_0^{\bar{z}} d\bar{s}_1 \sum_{h_1} \int d(\bar{\nu}_1) e^{i(h_1+2\rho\bar{\nu}_1)\theta_1^{(0)}} a_{h_1}(\bar{\nu}_1, \bar{\boldsymbol{x}}_1^{(0)}, \bar{s}_1) \frac{\partial}{\partial \bar{\boldsymbol{\eta}}} \times \cdots \times \int_0^{\bar{s}_{m-2}} d\bar{s}_{m-1} \\ & \times \sum_{h_{m-1}} \int d(\bar{\nu}_{m-1}) \exp i(h_{m-1}+2\rho\bar{\nu}_{m-1}) \theta_{m-1}^{(0)} a_{h_{m-1}}(\bar{\nu}_{m-1}, \bar{\boldsymbol{x}}_{m-1}^{(0)}, \bar{s}_{m-1}) \frac{\partial}{\partial \bar{\boldsymbol{\eta}}} \\ & \times \left[\hat{f}_0(\bar{s}_{m-1}, \theta_{m-1}^{(0)}, \bar{\boldsymbol{\eta}}, \bar{\boldsymbol{x}}_{m-1}^{(0)}, \bar{\boldsymbol{p}}_{m-1}^{(0)}) + \int_0^{\bar{s}_{m-1}} d\bar{s}_m \sum_{h_m} \int d(\bar{\nu}_m) \right. \\ & \left. \times e^{i(h_m+2\rho\bar{\nu}_m)\theta_m^{(0)}} a_{h_m}(\bar{\nu}_m, \bar{\boldsymbol{x}}_m^{(0)}, \bar{s}_m) \frac{\partial}{\partial \bar{\boldsymbol{\eta}}} \bar{f}_0(\bar{s}_m, \theta_m^{(0)}, \bar{\boldsymbol{\eta}}, \bar{\boldsymbol{x}}_m^{(0)}, \bar{\boldsymbol{p}}_m^{(0)}) \right]. \end{aligned} \tag{33}$$

Here

$$\begin{aligned} \theta_m^{(0)} &= \theta + \phi(\bar{s}_m - \bar{z}), \\ \bar{\boldsymbol{x}}_m^{(0)} &= \bar{\boldsymbol{x}} \cos[\bar{k}_\beta(\bar{s}_m - \bar{z})] + \frac{\bar{\boldsymbol{p}}}{\bar{k}_\beta} \sin[\bar{k}_\beta(\bar{s}_m - \bar{z})], \\ \bar{\boldsymbol{p}}_m^{(0)} &= -\bar{k}_\beta \bar{\boldsymbol{x}} \sin[\bar{k}_\beta(\bar{s}_m - \bar{z})] + \bar{\boldsymbol{p}} \cos[\bar{k}_\beta(\bar{s}_m - \bar{z})]. \end{aligned} \tag{34}$$

Inserting Eq. (33) into Eq. (19) and integrating over θ, we obtain

$$\begin{aligned} \left(\frac{\partial}{\partial \bar{z}} + i\bar{\nu}_h + \frac{\boldsymbol{\nabla}_\perp^2}{2ih} \right) a_h = & \left(\frac{K_h}{K_1} \right)^2 \int d^2\bar{p} \int d\bar{\eta} \sum_{h's} \int_0^{\bar{z}} d\bar{s}_1 e^{ih_1\phi(\bar{s}_1 - \bar{z})} \int d(\bar{\nu}_1) a_{h_1}(\bar{\nu}_1, \bar{\boldsymbol{x}}_1, \bar{s}_1) \frac{\partial}{\partial \bar{\boldsymbol{\eta}}} \times \cdots \\ & \times \int_0^{\bar{s}_{m-2}} d\bar{s}_{m-1} \int d(\bar{\nu}_{m-1}) a_{h_{m-1}}(\bar{\nu}_{m-1}, \bar{\boldsymbol{x}}_{m-1}, \bar{s}_{m-1}) \frac{\partial}{\partial \bar{\boldsymbol{\eta}}} \left[\hat{f}_{0,h_m} + \int_0^{\bar{s}_{m-1}} d\bar{s}_m \right. \\ & \left. \times e^{ih_m\phi(\bar{s}_m - \bar{z})} \int d(\bar{\nu}_m) a_{h_m}(\bar{\nu}_m, \bar{\boldsymbol{x}}_m, \bar{s}_m) \frac{\partial \bar{f}_0}{\partial \bar{\boldsymbol{\eta}}} \right] \delta(-\bar{\nu}_h + \bar{\nu}_1 + \cdots + \bar{\nu}_m), \end{aligned} \tag{35}$$

where the sum over *hs* consists of all harmonic interactions that satisfy $h_1 + \cdots + h_m = h$. Among them, the term with $h_m = h$ and all other h's equal to zero, gives rise to Eq. (25).

Let us estimate the relative strengths of harmonic fields generated from the process of self-amplified spontaneous emission. The general solution of Eq. (35) can be written as

$$a_h = a_h^L + a_h^{NL}, \tag{36}$$

where the linear harmonic field a_h^L is given by the second term of Eq. (27), and the nonlinear harmonic field a_h^{NL} is the solution due to the nonlinear harmonic interactions. Assume that $|\int d\bar{\nu}_h e^{i\nu\theta} a_h| \ll |\int d\bar{\nu}_1 e^{i\nu\theta} a_1| < 1$ for $|h|>1$, we have $a_1 \approx a_1^L \gg a_1^{NL}$ before saturation. For $|h|>1$, a_h^L does not grow much from the spontaneous emission as shown in Sec. III. Thus, the nonlinear interacting terms of Eq. (35) can be separated into two groups: those consisting of at least one $a_h^L(|h|>1)$ or $\hat{f}_{0,h}$ would generate nonlinear harmonics below the level of spontaneous harmonic emissions and can be ignored, and those consisting of interactions among a_1 and $a_h^{NL}(|h|>1)$ may generate more harmonic radiation than the linear harmonic generation. If we further postulate that a_h^{NL} is an $|h|^{th}$ order quantity, i.e.,

$$a_h^{NL} \sim a_1^{|h|}, \qquad \text{for} \quad |h|>1, \tag{37}$$

then we obtain from Eq. (35) that

$$a_h^{NL} \sim \sum_{h_1 + \cdots + h_m = h} a_1^{|h_1| + \cdots + |h_m|}. \tag{38}$$

To be consistent with Eq. (37), we drop higher-order (than the hth order) terms of a_h^{NL} by restricting the sum in Eq. (38) to those with $0<h_1,\ldots,h_m\leqslant h$. Thus, we conclude that the dominant nonlinear harmonic field is determined by all lower nonlinear harmonic fields as well as the fundamental field.

For instance, since both the fundamental and the third harmonic of a SASE FEL start with effective noises on the order of $1/\sqrt{N_e}$, we have

$$|a_3^L|\sim\frac{1}{\sqrt{N_e}}e^{\mathrm{Im}(\mu_3)\bar{z}},\quad |a_3^{NL}|\sim|a_1|^3\sim\left(\frac{1}{\sqrt{N_e}}e^{\mathrm{Im}(\mu_1)\bar{z}}\right)^3.$$

If $\mathrm{Im}(\mu_3)\ll\mathrm{Im}(\mu_1)$, then

$$a_3\approx\begin{cases} a_3^L & \text{when}\quad \bar{z}<\frac{2}{3}\bar{z}_{\mathrm{sat}} \\ a_3^{NL} & \text{when}\quad \bar{z}>\frac{2}{3}\bar{z}_{\mathrm{sat}} \end{cases} \tag{39}$$

where $\bar{z}_{\mathrm{sat}}\sim(\ln N_e)/2\,\mathrm{Im}(\mu_1)$ is the saturation length. Thus, when $\bar{z}>(2/3)\bar{z}_{\mathrm{sat}}$, the third-harmonic radiation is completely driven by the third power of the fundamental radiation, with a characteristic growth rate three times that of the fundamental. At the fifth harmonic, the leading nonlinear terms are $a_1^2a_3^{NL}$ and a_1^5. Since $a_3^{NL}\sim a_1^3$, both terms of a_5^{NL} are of the same order as a_1^5 and are the dominant components for a_5 after $\bar{z}>(4/5)\bar{z}_{\mathrm{sat}}$ in a SASE FEL. For a high-gain FEL where a bunch density modulation or a seed laser at the fundamental wavelength is present, the nonlinear interactions become dominant over the linear interaction for higher harmonics at a much earlier stage of the exponential growth regime. Hence we come to the conclusion that the dominant nonlinear terms for a_h^{NL} are eventually of the same order as $a_1^{|h|}$ for $|h|>1$, with a growth rate given by $|h|\,\mathrm{Im}(\mu_1)$. Such a growth rate scaling was first pointed out using a 1D model [3,17] and was observed up to the ninth harmonic using a three-dimensional simulation code [4]. Here we present a 3D analysis for this scaling by taking into account all possible harmonic interactions. In passing, we note that this perturbation analysis is not very accurate when $\bar{z}$ is too close to $\bar{z}_{\mathrm{sat}}$.

V. THIRD-HARMONIC GENERATION

In this section, we calculate explicitly the nonlinear harmonic generation for a_3^{NL}. The governing equation is obtained by setting $h=3$ and $h_1=h_2=h_3=1$ in Eq. (35):

$$\begin{aligned}
&\left(\frac{\partial}{\partial\bar{z}}+i\bar{\nu}_3+\frac{\bar{\nabla}_\perp^2}{6i}\right)a_3^{NL}(\bar{\nu}_3,\overline{\mathbf{x},z})-\left(\frac{K_3}{K_1}\right)^2\int d^2\bar{p}\int d\bar{\eta}\int_0^{\bar{z}}d\bar{s}_1e^{i3\phi(\bar{s}_1-\bar{z})}a_3^{NL}(\bar{\nu}_3,\bar{\mathbf{x}}_1^{(0)},\bar{s}_1)\frac{\partial\bar{f}_0}{\partial\bar{\eta}}\\
&=\left(\frac{K_3}{K_1}\right)^2\int d^2\bar{p}\int d\bar{\eta}\int_0^{\bar{z}}d\bar{s}_1e^{i\phi(\bar{s}_1-\bar{z})}\int d(\bar{\nu}_{1\alpha})a_1(\bar{\nu}_{1\alpha},\bar{\mathbf{x}}_1^{(0)},\bar{s}_1)\frac{\partial}{\partial\bar{\eta}}\\
&\times\int_0^{\bar{s}_1}d\bar{s}_2e^{i\phi(\bar{s}_2-\bar{z})}\int d(\bar{\nu}_{1\beta})a_1(\bar{\nu}_{1\beta},\bar{\mathbf{x}}_2^{(0)},\bar{s}_2)\frac{\partial}{\partial\bar{\eta}}\int_0^{\bar{s}_2}d\bar{s}_3e^{i\phi(\bar{s}_3-\bar{z})}\\
&\times\int d(\bar{\nu}_{1\gamma})a_1(\bar{\nu}_{1\gamma},\bar{\mathbf{x}}_3^{(0)},\bar{s}_3)\delta(-\bar{\nu}_3+\bar{\nu}_{1\alpha}+\bar{\nu}_{1\beta}+\bar{\nu}_{1\gamma})\frac{\partial\bar{f}_0}{\partial\bar{\eta}},
\end{aligned}\tag{40}$$

where the fundamental field is solved in Eq. (27) as

$$\begin{aligned}
a_1(\bar{\nu}_1,\overline{\mathbf{x},z})\propto e^{-i\mu_1\bar{z}}A_1(\bar{\mathbf{x}})\Bigg[&\int d^2\bar{\mathbf{x}}'A_1(\bar{\mathbf{x}}')a_{0,1}(\bar{\nu}_1,\bar{\mathbf{x}}')\\
&+\int d^2\bar{x}'\int d^2\bar{p}\int d\bar{\eta}\hat{f}_{0,1}(\bar{\nu}_1,\bar{\mathbf{x}}',\bar{\mathbf{p}},\bar{\eta})\\
&\times\int_{-\infty}^0 d\tau A_1(\bar{\mathbf{x}}^{(0)})e^{i(\phi-\mu_1)\tau}\Bigg].
\end{aligned}\tag{41}$$

Thus, the properties of the third nonlinear harmonic are completely specified by those of the fundamental. In the following, we discuss these properties for both coherent amplification and self-amplified spontaneous emission.

A. Coherent amplification

For FEL's that start with a coherent input (including the HGHG FEL's), the fundamental radiation has a well-defined frequency that is determined by the initial condition. Thus, we can drop the frequency dependence of a_1 and a_3^{NL} in Eq. (40). Assuming that the FEL operates at the optimal detuning $\bar{\nu}_0$ for the fundamental field (with a growth rate μ_0 that has the maximum imaginary part), we have $\bar{\nu}_{1\alpha}=\bar{\nu}_{1\beta}=\bar{\nu}_{1\gamma}=\bar{\nu}_0$ and $\bar{\nu}_3=3\bar{\nu}_0$. Equation (40) becomes

$$\begin{aligned}
&\left(\frac{\partial}{\partial\bar{z}}+3i\bar{\nu}_0+\frac{\bar{\nabla}_\perp^2}{6i}\right)a_3^{NL}(\overline{\mathbf{x},z})-\left(\frac{K_3}{K_1}\right)^2\int d^2\bar{p}\int d\bar{\eta}\\
&\times\int_0^{\bar{z}}d\bar{s}_1e^{3i\phi(\bar{s}_1-\bar{z})}a_3^{NL}(\bar{\mathbf{x}}_1^{(0)},\bar{s}_1)\frac{\partial\bar{f}_0}{\partial\bar{\eta}}\\
&=\left(\frac{K_3}{K_1}\right)^2\int d^2\bar{p}\int d\bar{\eta}\int_0^{\bar{z}}d\bar{s}_1e^{i\phi(\bar{s}_1-\bar{z})}a_1(\bar{\mathbf{x}}_1^{(0)},\bar{s}_1)\\
&\times\frac{\partial}{\partial\bar{\eta}}\int_0^{\bar{s}_1}d\bar{s}_2\times e^{i\phi(\bar{s}_2-\bar{z})}a_1(\bar{\mathbf{x}}_2^{(0)},\bar{s}_2)\frac{\partial}{\partial\bar{\eta}}
\end{aligned}$$

$$\times \int_0^{\bar{s}_2} d\bar{s}_3 e^{i\phi(\bar{s}_3-\bar{z})} a_1(\bar{\mathbf{x}}_3^{(0)},\bar{s}_3)\frac{\partial \bar{f}_0}{\partial \bar{\eta}}.$$

In view of Eq. (41), we write $a_1(\bar{\mathbf{x}},\bar{z})=e^{-i\mu_0\bar{z}}A_1(\bar{\mathbf{x}})$, where $A_1\approx A_0 e^{-w_1\bar{x}^2/\bar{\sigma}_x^2}$ is the guided mode using the Gaussian approximation [5], and A_0 is the appropriate normalization coefficient. Thus, we can write the third nonlinear harmonic $a_3^{NL}=e^{-3i\mu_0 z}A_3^{NL}$ with the transverse profile A_3^{NL} by:

$$\left[-3i(\mu_0-\bar{\nu}_0)+\frac{\bar{\nabla}_\perp^2}{6i}\right]A_3^{NL}(\bar{\mathbf{x}})-\left(\frac{K_3}{K_1}\right)^2\int d^2\bar{p}\int d\bar{\eta}$$
$$\times\int_{-\infty}^0 d\tau_1 A_3^{NL}(\bar{\mathbf{x}}_1^{(0)})e^{3i(\phi-\mu_0)\tau_1}\frac{\partial \bar{f}_0}{\partial\bar{\eta}}$$
$$=\left(\frac{K_3}{K_1}\right)^2\int d^2\bar{p}\int d\bar{\eta}\int_{-\infty}^0 d\tau_1 e^{3i(\phi-\mu_0)\tau_1}A_1(\bar{\mathbf{x}}_1^{(0)})\frac{\partial}{\partial\bar{\eta}}$$
$$\times\int_{-\infty}^0 d\tau_2\times e^{2i(\phi-\mu_0)\tau_2}A_1(\bar{\mathbf{x}}_2^{(0)})\frac{\partial}{\partial\bar{\eta}}$$
$$\times\int_{-\infty}^0 d\tau_3 e^{i(\phi-\mu_0)\tau_3}A_1(\bar{\mathbf{x}}_3^{(0)})\frac{\partial\bar{f}_0}{\partial\bar{\eta}}, \tag{43}$$

where $\tau_m=\bar{s}_m-\bar{s}_{m-1}$ for $m=1,2,3$ and $\bar{s}_0=\bar{z}$. We have extended the lower limit of the integral $\int d\tau_m$ to $-\infty$ due to the exponential growth of the field amplitudes. The left-hand side of Eq. (43) is the same as Eq. (26) for $h=3$, except we replace μ_3 by $3\mu_0$ and $\bar{\nu}_3$ by $3\bar{\nu}_0$. Following the matrix formulation for the left-hand side of Eq. (43) and carrying out $\int d^2\bar{p}\int d\bar{\eta}$ for the right-hand side, we arrive at

$$[\mathbf{I}-\mathbf{T}_3(3\mu_0)]\mathbf{A}_3^{NL}=\left(\frac{K_3}{K_1}\right)^2 A_0^3\mathbf{H} \tag{44}$$

in the Hankel transformed Q space, where the nth element of the vector $\mathbf{H}$ is

$$H_n=\frac{-1/w_1^2}{12(\mu_0-\bar{\nu}_0)-2Q_n^2/(3\bar{\sigma}_x^2)}\int_{-\infty}^0 d\tau_1\int_{-\infty}^0 d\tau_2\int_{-\infty}^0 d\tau_3$$
$$\times\frac{3\tau_1(3\tau_1+2\tau_2)(3\tau_1+2\tau_2+\tau_3)}{U}$$
$$\times\exp\left[-\frac{\bar{\sigma}_\eta^2}{2}(3\tau_1+2\tau_2+\tau_3)^2\right.$$
$$\left.-i\mu_0(3\tau_1+2\tau_2+\tau_3)-\frac{Q_n^2}{4w_1 S}\right], \tag{45}$$

and

$$S=\frac{U}{V+\Sigma_{m=1,2,3}\sin^2(\bar{k}_\beta\Sigma_{l=1}^m\tau_l)},$$

$$U=\left[\sum_{m=1}^3\sin^2\left(\bar{k}_\beta\sum_{l=1}^m\tau_l\right)\right]\left[\sum_{m=1}^3\cos^2\left(\bar{k}_\beta\sum_{l=1}^m\tau_l\right)\right]$$
$$-\left[\sum_{m=1}^3\sin\left(\bar{k}_\beta\sum_{l=1}^m\tau_l\right)\cos\left(\bar{k}_\beta\sum_{l=1}^m\tau_l\right)\right]^2+V^2+3V,$$

$$V=\frac{1}{2w_1}+\frac{i}{2w_1}\bar{k}_\beta^2\bar{\sigma}_x^2(3\tau_1+2\tau_2+\tau_3). \tag{46}$$

We can ignore $\mathbf{T}_3(3\mu_0)$ with respect to the identity matrix because the linear harmonic generation is much weaker compared to the nonlinear generation. The transverse profile for the third nonlinear harmonic is obtained after Hankel transforming the solution of Eq. (44) and is approximately Gaussian in R, i.e.,

$$A_3^{NL}(R)\approx\left(\frac{K_3}{K_1}\right)^2 A_0^3\int QdQJ_0(QR)H(Q)$$
$$\approx\left(\frac{K_3}{K_1}\right)H_0 A_0^3 e^{-w_3R^2}. \tag{47}$$

Thus, the third nonlinear harmonic is also transversely coherent. In general, the transverse mode size of the third nonlinear harmonic is always narrower than that of the fundamental due to the nonlinear generation mechanism (see numerical examples with Figs. 1 and 3 in Sec. VI).

B. Self-amplified spontaneous emission

For a SASE FEL, the fundamental radiation starts with a white-noise spectrum and has a finite gain bandwidth. It is convenient to solve for the slowly varying electric field $\tilde{a}_3(\bar{\theta})=\int d\bar{\nu}_3 e^{i\bar{\nu}_3\bar{\theta}}a_3(\bar{\nu}_3)$ along the scaled bunch position $\bar{\theta}=2\rho\theta$ and write Eq. (40) as

$$\left(\frac{\partial}{\partial\bar{z}}+\frac{\partial}{\partial\bar{\theta}}+\frac{\bar{\nabla}_\perp^2}{6i}\right)\tilde{a}_3^{NL}-\left(\frac{K_3}{K_1}\right)^2\int d^2\bar{p}\int d\bar{\eta}\int_0^{\bar{z}}d\bar{s}_1 e^{3i\phi(\bar{s}_1-\bar{z})}\tilde{a}_3^{NL}(\bar{\theta},\bar{\mathbf{x}}_1^{(0)},\bar{s}_1)\frac{\partial\bar{f}_0}{\partial\bar{\eta}}$$
$$=\left(\frac{K_3}{K_1}\right)^2\int d^2\bar{p}\int d\bar{\eta}\int_0^{\bar{z}}d\bar{s}_1 e^{i\phi(\bar{s}_1-\bar{z})}\tilde{a}_1(\bar{\theta},\bar{\mathbf{x}}_1^{(0)},\bar{s}_1)\frac{\partial}{\partial\bar{\eta}}\int_0^{\bar{s}_1}d\bar{s}_2 e^{i\phi(\bar{s}_2-\bar{z})}$$
$$\times\tilde{a}_1(\bar{\theta},\bar{\mathbf{x}}_2^{(0)},\bar{s}_2)\frac{\partial}{\partial\bar{\eta}}\int_0^{\bar{s}_2}d\bar{s}_3 e^{i\phi(\bar{s}_3-\bar{z})}\tilde{a}_1(\bar{\theta},\bar{\mathbf{x}}_3^{(0)},\bar{s}_3)\frac{\partial f_0}{\partial\bar{\eta}}. \tag{48}$$

In the absence of an external signal, we drop the first term in Eq. (41) and perform the Fourier transformation of the second term. In order to estimate the average power of the third nonlinear harmonic, we make the following simplifying assumption about $\tilde{a}_1$ in the exponential regime.

$$\tilde{a}_1(\bar{\theta},\bar{\mathbf{x}},\bar{z}) \approx e^{-i\mu_0\bar{z}+i\bar{\nu}_0\bar{\theta}} A_0 e^{-w_1\bar{x}^2/\bar{\sigma}_x^2} \sum_{j=1}^{N} e^{-i\theta_j} g_1(\bar{\theta}-\bar{\theta}_j,\bar{z}). \tag{49}$$

Here $g_1(\bar{\theta}-\bar{\theta}_j,\bar{z})$ is the longitudinal Green's function whose variation in $\bar{z}$ and $\bar{\theta}$ is much slower than the exponential variation in Eq. (49) (see Appendix B for more discussion). Writing $\tilde{a}_3^{NL}=e^{-3i\mu_0\bar{z}+3i\bar{\nu}_0\bar{\theta}}\tilde{A}_3^{NL}(\bar{\mathbf{x}},\bar{z},\bar{\theta})$ and assuming that $\tilde{A}_3^{NL}$ depends only weakly on $\bar{z}$ and $\bar{\theta}$, the equation for $\tilde{A}_3^{NL}$ is then very similar to Eq. (43). Following the derivation of Sec. V A, we obtain

$$\begin{aligned}\tilde{A}_3^{NL} &\approx \left(\frac{K_3}{K_1}\right)^2 A_0^3 G_1^3 \int Q dQ J_0(QR) H(Q) \\ &\approx \left(\frac{K_3}{K_1}\right) H_0 A_0^3 e^{-w_3 R^2} G_1^3,\end{aligned} \tag{50}$$

where $G_1=\Sigma_{j=1}^{N} e^{-i\theta_j} g_1(\bar{\theta}-\bar{\theta}_j,\bar{z})$ can be regarded as a random phasor sum and $H(Q)$ is described in Eq. (45). Hence, the third nonlinear harmonic radiation is transversely coherent and longitudinally chaotic, similar to the fundamental radiation in SASE FEL. However, the spikes of the third harmonic become more pronounced due to the third-power dependence on the random variable G_1, implying higher average value (than the corresponding steady-state case) and more shot-to-shot fluctuations for the total radiation energy. The statistical properties of the third nonlinear harmonic radiation are discussed in Appendix B.

In both cases, since the instantaneous third-harmonic radiation intensity is

$$I_3 = \rho I_{\text{beam}} \left| \left(\frac{K_1}{K_3}\right) \tilde{a}_3 \right|^2 = \rho I_{\text{beam}} e^{6\,\text{Im}(\mu_0)\bar{z}} \left(\frac{K_1}{K_3}\right)^2 |\tilde{A}_3^{NL}(R)|^2, \tag{51}$$

the average power of the third-harmonic radiation is given by

$$\begin{aligned}P_3^{NL} &= \int dx dy \langle I_3 \rangle \\ &= e^{6\,\text{Im}(\mu_0)\bar{z}} \rho I_{\text{beam}} 2\pi\sigma_x^2 \left(\frac{K_1}{K_3}\right)^2 \int R dR \langle |\tilde{A}_3^{NL}(R)| \rangle \\ &= \rho P_{\text{beam}} e^{6\,\text{Im}(\mu_0)\bar{z}} \frac{A_0^6 |H_0|^2}{4 w_{3r}} \times \begin{cases} 1 & \text{CA}, \\ \langle G_1^3 (G_1^3)^* \rangle & \text{SASE}, \end{cases}\end{aligned} \tag{52}$$

where $P_{\text{beam}}=2\pi\sigma_x^2 I_{\text{beam}}$ is the total electron-beam power, and w_{3r} is the real part of w_3. Similarly, we write the fundamental power as

$$P_1 = \rho P_{\text{beam}} e^{2\,\text{Im}(\mu_0)\bar{z}} \frac{A_0^2}{4 w_{1r}} \begin{cases} 1 & \text{CA}, \\ \langle G_1 G_1^* \rangle & \text{SASE}, \end{cases} \tag{53}$$

where w_{1r} is again the real part of w_1. Using Eqs. (53) and (B8), we simplify Eq. (52) as

$$\left(\frac{P_3^{NL}}{\rho P_{\text{beam}}}\right) \approx |H_0|^2 \frac{16 w_{1r}^3}{w_{3r}} \left(\frac{P_1}{\rho P_{\text{beam}}}\right)^3 \times \begin{cases} 1 & \text{CA}, \\ 6 & \text{SASE}, \end{cases} \tag{54}$$

VI. NUMERICAL EXAMPLES

In this section, we illustrate the analytical results of the previous sections using two current high-gain FEL projects. The first example is motivated by Ref. [4], where the steady-state simulation of up to the ninth harmonic is performed for the low-energy undulator test line (LEUTL) FEL at the advanced photon source [18]. The nominal parameters for the LEUTL FEL are listed in Table I, from which we find $\bar{\sigma}_x=0.56$, $\bar{\sigma}_\eta=0.25$, and $\bar{k}_\beta=0.46$ for our scaled parameters. Using the matrix formulation of Sec. III, the complex growth rates of the fundamental and the third linear harmonic are $\mu_0=-0.42+0.5i$ (at the optimal detuning $\bar{\nu}_0=-0.42$) and $(\mu_3)_0=-0.87+0.16i$ [at $(\bar{\nu}_3)_0=-0.87$], and the transverse mode calculation yields the guided mode with $w_1=0.16-0.093i$. Thus, the linear part of the third-harmonic radiation grows much slower than the fundamental radiation. Nevertheless, the third nonlinear harmonic grows three times as fast as the fundamental and can dominate over the linear part. In order to compare with Ref. [4], which starts the MEDUSA simulation using a seed laser at the fundamental, we employ the formulas of coherent amplification for the nonlinear harmonic calculation even though the LEUTL experiment starts from shot noise. We find that $w_{3r}=0.39$ and $|H_0|^2=1.4$ and plot the transverse profiles of the third nonlinear harmonic, the fundamental, and the electron beam in Fig. 1. Note that the third-harmonic radiation is guided in the exponential regime, with a smaller spot size than that of the fundamental due to the nonlinear generation mechanism. This behavior is different from the MEDUSA simulation [4] that shows the spot sizes of higher harmonics expand initially and focus rapidly in the latter stage of the interaction. In the exponential growth regime, the third nonlinear harmonic power P_3^{NL} is obtained from Eq. (54):

$$\frac{P_3^{NL}}{\rho P_{\text{beam}}} = 0.24 \left(\frac{P_1}{\rho P_{\text{beam}}}\right)^3$$

for LEUTL FEL (steady-state mode), (55)

where $\rho P_{\text{beam}}=130$ MW. Using the fitting formula of the saturation power $P_{\text{sat}} \approx 2.1[\text{Im}(\mu_0)]^2 \rho P_{\text{beam}}=70$ MW for the fundamental [19] and assuming that Eq. (55) is valid till $P_1=P_{\text{sat}}/2=35$ MW, we estimate that the third-harmonic power can reach the 600 kW level. The MEDUSA simulation [4] shows the saturated third-harmonic power at 2.67 MW. In Fig. 2, we plot the third-harmonic power as a function of the undulator distance z, calculated from Eq. (55) with P_1 given by the MEDUSA simulation. It agrees with the MEDUSA third-harmonic power level.

In the second example, we consider the proposed x-ray FEL linac coherent light source (LCLS) at Stanford Linear Accelerator Center [20]. Using the current LCLS design parameters in Table I, we have $\bar{\sigma}_x=2.8$, $\bar{\sigma}_\eta=0.45$, and $\bar{k}_\beta=0.29$. The fundamental guided mode has a complex growth

TABLE I. Third-harmonic computation for the LEUTL FEL and the LCLS project.

	LEUTL (steady state)	LCLS ($\lambda_r = 1.5$ Å)	LCLS ($\lambda_r = 4.5$ Å)
e-beam and undulator			
energy	220 MeV	14.4 GeV	8.3 GeV
peak current	150 A	3400 A	3400 A
normalized emittance	5 μm	1.5 μm	3 μm
energy spread	0.1%	0.02%	0.02%
average beta function	1.5 m	18 m	18 m
undulator period	3.3 cm	3 cm	3 cm
undulator strength	3.1	3.71	3.71
fundamental wavelength	518 nm	1.5 Å	4.5 Å
Calculated FEL properties			
fundamental power gain length	0.67 m	6.1 m	5.0 m
fundamental saturation power	70 MW	8 GW	7 GW
third-harmonic power (P_3)[a]	600 kW	15 MW	40 MW
third-harmonic bunching (b_3)[b]	0.3	0.02	0.04
Simulation comparison			
MEDUSA saturated P_3	2.67 MW		
GINGER saturated b_3	0.2	0.03	0.05

[a]Evaluated when the fundamental reaches one-half of the saturation power.
[b]Same as a.

rate $\mu_0 = -1.2 + 0.42i$ and a mode profile determined by $w_1 = 0.64 - 0.50i$ at the optimal detuning $\bar{\nu}_0 = -1.0$, consistent with the result of Ref. [5]. However, the linear growth rate of the third harmonic is almost zero at any detuning because the emittance and the energy spread of the beam is too large at this wavelength (0.5 Å) to have any linear amplification. Thus, the third-harmonic radiation is largely spontaneous in the first two-thirds of the full saturation length, until the nonlinear harmonic generation becomes prominent. The transverse profile of the third nonlinear harmonic is obtained from Eq. (47) and is shown in Fig. 3, with $w_{3r} = 1.4$ and $|H_0|^2 = 6.3 \times 10^{-3}$. In comparison, Fig. 3 also shows the electron-beam profile and the fundamental radiation mode in the exponential growth regime. Note that the spot size of the fundamental radiation is smaller than the electron-beam size because the effect of diffraction is quite small in the x-ray wavelength (in contrast to Fig. 1, the LEUTL case in the visible wavelength), and the spot size of the third nonlinear harmonic is smaller than that of the fundamental. In view of the so-called diffraction-limited criteria $\epsilon < \lambda_r/4\pi$ to generate transversely coherent radiation at wavelength λ_r, the requirement on the emittance ϵ is further violated by a factor of 3 at the third-harmonic wavelength [21], in addition to a factor of 4.5 at the fundamental wavelength due to the optical guiding of the electron beam [5]. Using Eq. (54) for SASE, we obtain the third-harmonic power P_3^{NL} from the nonlinear harmonic generation

$$\frac{P_3^{NL}}{\rho P_{\text{beam}}} = 0.11 \left(\frac{P_1}{\rho P_{\text{beam}}} \right)^3 \tag{56}$$

for LCLS. Here $\rho P_{\text{beam}} = 22$ GW with the current LCLS parameters. We take $P_1 = P_{\text{sat}}/2 \approx 4$ GW before the FEL saturation and estimate the third-harmonic power to be 15 MW. We also calculate the third-harmonic bunching parameter

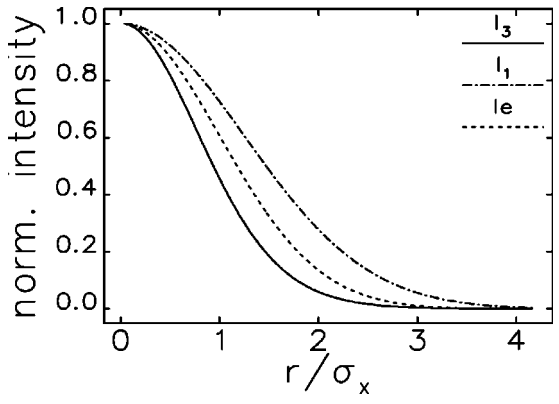

FIG. 1. Transverse profiles of the third harmonic (I_3), the fundamental radiation (I_1), and the electron beam (I_e) as functions of the radius in units of electron-beam size, using the LEUTL FEL parameters from Table I.

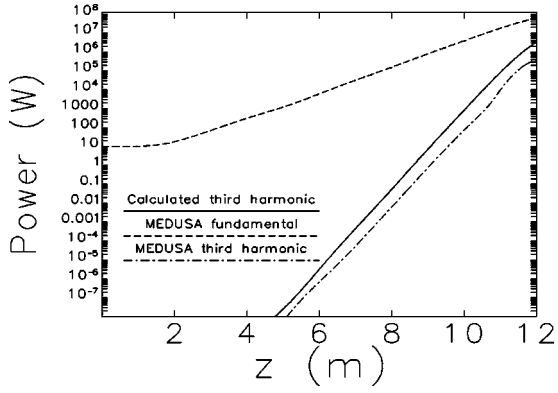

FIG. 2. Comparison of the calculated third-harmonic power and the MEDUSA steady-state simulation for the LEUTL FEL. The solid curve is calculated from Eq. (55) using the fundamental power obtained from MEDUSA (the dashed curve). The dotted curve is the third-harmonic power from the same simulation.

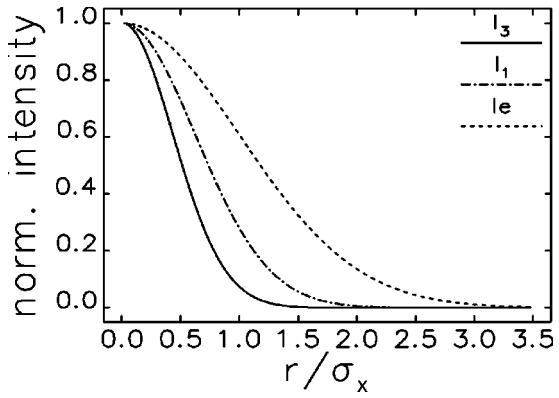

FIG. 3. Transverse profiles of the third harmonic (I_3), the fundamental radiation (I_1), and the electron beam (I_e) as functions of the radius in units of electron-beam size, using the LCLS ($\lambda_r = 1.5$ Å) parameters.

(defined in Appendix C) according to Eq. (C4) and compare with the GINGER simulation results in Fig. 4 for a steady-state GINGER run (coherent amplification) and Fig. 5 for a SASE run. Reasonable agreement is found in the exponential growth regime. In addition, as shown in Fig. 5, there is almost no linear growth of the third harmonic until the nonlinear harmonic generation becomes prominent above the noise level.

As another illustration, suppose we reduce the requirements on electron-beam energy and normalized emittance for LCLS to 8.3 GeV and 3 π mm mrad, respectively [22]. If we keep the same undulator parameters and other beam parameters (see Table I), the fundamental radiation wavelength becomes 4.5 Å. A similar calculation as above shows that the third-harmonic power at 1.5 Å can reach 40 MW when the power of the fundamental is one-half of the saturation power $P_{\mathrm{sat}} = 7$ GW. The peak brightness of this harmonic radiation is about 2×10^{30} photons/(s mm^2 mrad^2).

VII. CONCLUSION

In summary, both the linear and the nonlinear harmonic generation in a high-gain FEL are analyzed in perturbation

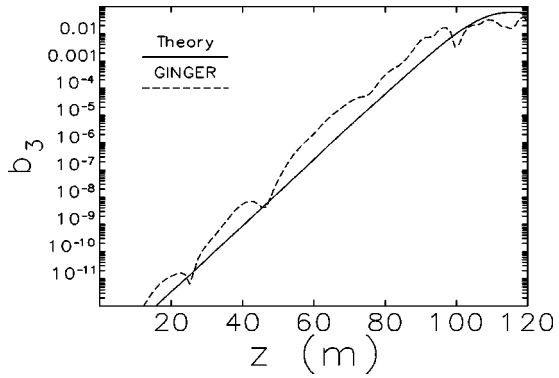

FIG. 4. Comparison of the calculated third-harmonic bunching and the GINGER steady-state simulation for LCLS. The solid curve is calculated from Eq. (C4) using the LCLS ($\lambda_r = 1.5$ Å) parameters and the fundamental power obtained from a single-frequency (optimal detuning) GINGER run. The dashed curve is the third-harmonic bunching output of the same run.

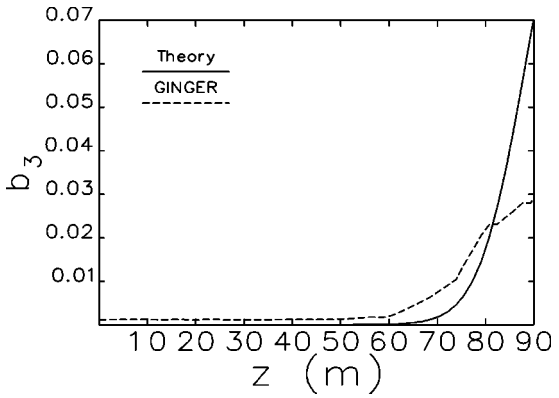

FIG. 5. Comparison of the calculated third-harmonic bunching and the GINGER SASE simulation for LCLS. The solid curve is calculated from Eq. (C4) using the LCLS ($\lambda_r = 1.5$ Å) parameters and the fundamental power obtained from GINGER SASE run. The dashed curve is the third-harmonic bunching output of the same run.

theory, including the effects due to energy spread, emittance, and betatron focusing of the electron beams, as well as the diffraction and optical guiding of the radiation field. Driven by the third power of the radiation field in the fundamental, the third nonlinear harmonic grows three times faster, is transversely coherent (with a smaller spot size), and has a significant power level for the LEUTL FEL and the LCLS project. Measurement of these nonlinear harmonics at the ongoing SASE FEL experiment [18] at Argonne National Laboratory and the HGHG experiment [23] at Brookhaven National Laboratory is planned [24]. Practical effects, such as undulator separation, misalignment, and magnetic-field errors to these nonlinear harmonics, are currently under study. As pointed out in Refs. [3,4] and fully analyzed here, the generation of nonlinear higher harmonics could be useful in extending the short-wavelength reach of a high-gain FEL.

ACKNOWLEDGMENTS

We thank S. Biedron, Y. Chae, W. Fawley, H. Freund, S. Milton, and C. Pelligrini for useful discussions. We also thank H. Freund for providing the MEDUSA simulation results shown in Fig. 2. Special thanks goes to W. Fawley for providing the latest version of the simulation code GINGER at ANL and for his generous assistance with running the code. This work was supported by the U.S. Department of Energy, Office of Basic Energy Sciences, through Contract No. W-31-109-ENG-38.

APPENDIX A: VAN KAMPEN'S NORMAL MODE EXPANSION

We illustrate Van Kampen's normal-mode expansion [25] by solving the initial value problem of the fundamental radiation field that is initiated by an external signal or by shot noise. This extends the treatment of Ref. [13] to the electron beam with finite emittance. First, we introduce the state vector

$$\Phi=\begin{pmatrix} a_\nu(\overline{x},\overline{z}) \\ f_\nu(\overline{x},\overline{p},\overline{\eta},\overline{z}) \end{pmatrix} \equiv \begin{pmatrix} a_1(\overline{\nu}_1,\overline{x},\overline{z}) \\ \int \frac{2\rho d\theta}{2\pi} e^{-i\nu\theta} f(\overline{x},\hat{\overline{p}},\overline{\eta},\theta,\overline{z}) \end{pmatrix}, \tag{A1}$$

where f_ν satisfies the linearized Vlasov equation

$$\frac{\partial f_\nu}{\partial \overline{z}} + i\nu\phi f_\nu + \dot{\overline{x}}\frac{\partial f\nu}{\partial \overline{x}} + \dot{\overline{p}}\frac{\partial f\nu}{\partial \overline{p}} - a_\nu \frac{\partial \overline{f_0}}{\partial \overline{\eta}} = 0, \tag{A2}$$

and $\overline{f}_0(\overline{p}^2+\overline{k}_\beta^2\overline{x}^2,\overline{\eta})$ is the smooth background distribution of a matched, coasting beam. Combining Eq. (A2) with the scaled Maxwell Eq. (19), one can write

$$\left(\frac{\partial}{\partial \overline{z}} - i\mathbf{M}\right)\Phi = 0, \tag{A3}$$

where

$$\mathbf{M}\Phi(\overline{z}) = \begin{pmatrix} \left(-\overline{\nu}_1 + \frac{\boldsymbol{\nabla}_\perp^2}{2}\right)a_\nu - i\int d^2\overline{p}\int d\overline{\eta} f_\nu \\ -ia_\nu \frac{\partial \overline{f_0}}{\partial \overline{\eta}} + \left[-\nu\phi + i\left(\dot{\overline{x}}\frac{\partial}{\partial \overline{\mathbf{x}}} + \dot{\overline{\mathbf{p}}}\frac{\partial}{\partial \overline{\mathbf{p}}}\right)\right] f_\nu \end{pmatrix}. \tag{A4}$$

The scalar product of two state vectors is defined by

$$(\Phi_1,\Phi_2) \equiv \int d^2\overline{x} a_{1\nu} a_{2\nu} + \int d^2\overline{x}\int d^2\overline{p}\int d\overline{\eta} f_{1\nu} f_{2\nu}. \tag{A5}$$

Let us assume the solution of the form

$$e^{-i\mu\overline{z}} = e^{-i\mu\overline{z}}\begin{pmatrix} A(\overline{x}) \\ \mathcal{F}(\overline{x},\overline{p},\overline{\eta}) \end{pmatrix}. \tag{A6}$$

Equation (A3) becomes the eigenvalue equation:

$$(\mu_n+\mathbf{M})\Psi_n = 0, \text{ or } \begin{pmatrix} \mu_n A_n + \left(-\overline{\nu}_1 + \frac{\boldsymbol{\nabla}_\perp^2}{2}\right)A_n - i\int d^2\overline{p}\int d\overline{\eta}\mathcal{F}_n \\ \mu_n\mathcal{F}_n - iA_n\frac{\partial \overline{f_0}}{\partial \overline{\eta}} + \left[-\nu\phi + i\left(\dot{\overline{x}}\frac{\partial}{\partial \overline{\mathbf{x}}} + \dot{\overline{\mathbf{p}}}\frac{\partial}{\partial \overline{\mathbf{p}}}\right)\right]\mathcal{F}_n \end{pmatrix} = 0. \tag{A7}$$

Here n indicates a discrete set of eigenvalues and eigenvectors. The second row of Eq. (A7) can be integrated to give

$$\mathcal{F}_n = \frac{\partial \overline{f_0}}{\partial \overline{\eta}}\int_{-\infty}^{0} d\tau A_n(\overline{\mathbf{x}}^{(0)}) e^{i(\nu\phi-\mu_n)\tau}, \tag{A8}$$

where $\overline{\mathbf{x}}^{(0)} = \overline{\mathbf{x}}\cos\overline{k}_\beta\tau + (\overline{\mathbf{p}}/k_\beta)\sin\overline{k}_\beta\tau$. Substituting this into the first row of Eq. (A7), we obtain the mode equation for the fundamental radiation

$$\left(-i\mu_n + i\overline{\nu}_1 + \frac{\boldsymbol{\nabla}_\perp^2}{2i}\right)A_n(\overline{\mathbf{x}}) - \int d^2\overline{p}\int d\overline{\eta}\int_{-\infty}^{0} d\tau A_n(\overline{\mathbf{x}}^{(0)}) e^{i(\nu\phi-\mu_n)\tau}\frac{d\overline{f_0}}{d\overline{\eta}} = 0. \tag{A9}$$

One can solve the mode equation numerically (as illustrated in Sec. III) to obtain the eigenvalue μ_n and the mode function A_n. $\mathcal{F}_n$ is then determined from Eq. (A8).

To form the orthogonal basis of these eigenvectors, consider the adjoint eigenvalue equation

$$(\mu_n^\dagger + \mathbf{M}^\dagger)\Psi_n^\dagger = 0. \tag{A10}$$

Here $\mu_n^\dagger$ and $\Psi_n^\dagger = (A_n^\dagger, F_n^\dagger)$ are the adjoint eigenvalues and eigenvectors of the adjoint operator $\tilde{\mathbf{M}}$, defined through

$$(\mathbf{M}^\dagger\Psi_n^\dagger,\Phi) = (\Psi_n^\dagger,\mathbf{M}\Phi). \tag{A11}$$

This leads to

$$\mathbf{M}^\dagger\Psi_n^\dagger = \begin{pmatrix} \left(-\overline{\nu}_1 + \frac{\boldsymbol{\nabla}_\perp^2}{2}\right)A_n^\dagger - i\int d^2\overline{p}\int d\overline{\eta}\frac{\partial \overline{f_0}}{\partial \overline{\eta}}F_n^\dagger \\ -iA_n^\dagger + \left[-\nu\phi + i\left(\dot{\overline{x}}\frac{\partial}{\partial \overline{\mathbf{x}}} + \dot{\overline{\mathbf{p}}}\frac{\partial}{\partial \overline{\mathbf{p}}}\right)\right]F_n^\dagger \end{pmatrix}. \tag{A12}$$

Putting this into Eq. (A10) and solving for $F_n^\dagger$ and $A_n^\dagger$, we find that

$$F_n^\dagger = \int_{-\infty}^{0} d\tau A_n^\dagger(\overline{\mathbf{x}}^{(0)}) e^{i(\nu\phi-\mu_n)\tau}, \tag{A13}$$

and that $A_n^\dagger$ satisfies the same mode equation as Eq. (A9). Hence we set $A_n^\dagger = A_n$ and $\mu_n^\dagger = \mu_n$.

By virtue of Eq. (A11), one immediately obtains

$$(\mu_n-\mu_m)(\Psi_m^\dagger,\Psi_n) = (\Psi_m^\dagger,\mathbf{M}\Psi_n) - (\mathbf{M}^\dagger\Psi_m^\dagger,\Psi_n) = 0. \tag{A14}$$

If these normal modes are not degenerate, i.e., $\mu_n \neq \mu_m$ for any $n \neq m$, the Van Kampen orthogonality for a discrete set of eigenvectors follows [25]:

$$(\Psi_m^\dagger,\Psi_n) = \delta_{m,n}(\Psi_n^\dagger,\Psi_n). \tag{A15}$$

Similarly, one can have orthogonality for a continuous set of eigenvectors using the Dirac δ function instead of the Kronecker delta function $\delta_{m,n}$ [25]. Furthermore, assuming the set of eigenvectors is complete, we can expand any state vector Φ as

$$\Phi(\bar{z})=\sum_n e^{-i\mu_n \bar{z}}\bar{C}_n\Psi_n=\sum_n e^{-i\mu_n \bar{z}}\frac{\bar{[}\Psi_n^\dagger,\Phi(0)]}{(\Psi_n^\dagger,\Psi_n)}\Psi_n. \tag{A16}$$

Here the initial state vector $\Phi(0)$ consists of the external signal $a_{0,\nu}$ and the νth Fourier component of the shot noise $\hat{f}_{0,\nu}$. Thus, we have

$$\begin{aligned}[\Psi_n^\dagger,\Phi(0)]=&\int d^2\bar{x}\bar{a}_{0,\nu}(\bar{\mathbf{x}})A_n(\bar{\mathbf{x}})\\&+\int d^2\bar{x}\int d^2\bar{p}\int d\bar{\eta}\hat{\bar{f}}_{0,\nu}(\bar{\mathbf{x}},\bar{\mathbf{p}},\bar{\eta})\\&\times\int_{-\infty}^0 d\tau A_n(\bar{\mathbf{x}}^{(0)})e^{i(\nu\phi-\mu_n)\tau},\end{aligned} \tag{A17}$$

and

$$\begin{aligned}(\Psi_n^\dagger,\Psi_n)=&\int d^2\bar{x}\bar{A}_n^2(\bar{\mathbf{x}})+\int d^2\bar{x}\int d^2\bar{p}\int d\bar{\eta}\frac{\partial\bar{f}_0}{\partial\bar{\eta}}\\&\times\left[\int_{-\infty}^0 d\tau A_n(\bar{\mathbf{x}}^{(0)})e^{i(\nu\phi-\mu_n)\tau}\right]^2.\end{aligned} \tag{A18}$$

After the completion of this paper, we heard a talk by M. Xie [26], who has independently obtained these results by an equivalent method.

APPENDIX B: STATISTICAL PROPERTIES OF THE THIRD NONLINEAR HARMONIC RADIATION IN SELF-AMPLIFIED SPONTANEOUS EMISSION

In this appendix, we study the statistical properties of the third nonlinear harmonic radiation in SAFE. The temporal structure of the fundamental radiation of SASE is essentially chaotic and has been discussed in Refs. [27] and [28]. For a monochromatic beam in the one-dimensional limit, the random distribution of wave packets is

$$\begin{aligned}G_1(\bar{\theta},\bar{z})=&\sum_{j=1}^{N_e} e^{-i\theta_j}g_1(\bar{\theta}-\bar{\theta}_j,z)\\=&\frac{G_0}{\sqrt{\bar{z}}}\sum_{j=1}^{N_e} e^{-i\theta_j}\exp\left[\frac{-\left(\bar{\theta}-\bar{\theta}_j+\frac{2}{3}\bar{z}\right)^2}{4\sigma_\theta^2(\bar{z})}\left(1-\frac{i}{\sqrt{3}}\right)\right],\end{aligned} \tag{B1}$$

where $\bar{\theta}=2\rho\theta$ and $\sigma_{\bar{\theta}}=(\bar{z}/18\sqrt{3})^{1/2}$ is the coherence length in units of $\lambda_r/(4\pi\rho)$. Since $\rho\ll 1$, the coherence length is normally much larger than the fundamental radiation wavelength λ_r in the exponential regime. G_1 is a random phasor sum of many Gaussian wave packets and its amplitude obeys the negative exponential probability [29]

$$P(|G_1|)=\frac{2|G_1|}{\bar{I}_1}\exp\left(-\frac{|G_1|^2}{\bar{I}_1}\right), \tag{B2}$$

where the average radiation ''intensity'' is

$$\begin{aligned}\bar{I}_1=\langle G_1G_1^*\rangle=&\frac{G_0}{\sqrt{\bar{z}}}\frac{N_e}{\bar{\theta}_b}\int_{-\bar{\theta}_b/2}^{\bar{\theta}_b/2}d\vartheta\exp\left(\frac{-gc^2}{2\sigma_{\bar{\theta}}^2}\right)\\=&\frac{G_0}{\sqrt{\bar{z}}}\frac{N_e}{\bar{\theta}_b}\sqrt{2\pi}\sigma_{\bar{\theta}}\end{aligned} \tag{B3}$$

for a flat-top bunch with scaled bunch length $\bar{\theta}_b\gg\sigma_{\bar{\theta}}$. The average value of the nth moment $|G_1|^n$ can be calculated as

$$\begin{aligned}\langle|G_1|^n\rangle=&\int_0^\infty|G_1|^n\frac{2|G_1|}{\bar{I}_1}\exp\left(-\frac{|G_1|^2}{\bar{I}_1}\right)d|G_1|\\=&\Gamma\left(\frac{n}{2}+1\right)\bar{I}_1^{n/2},\end{aligned} \tag{B4}$$

where $\Gamma(x)$ is the Euler gamma function.

The total radiation ''energy'' is integrated along the pulse and is given by $W_1=\int\bar{I}_1(\bar{\theta})d\bar{\theta}=\bar{I}_1\bar{\theta}_b$ for the flat-top bunch. The variance of the radiation energy is

$$\begin{aligned}\sigma_{W_1}^2=&\int_{-\bar{\theta}_b/2}^{\bar{\theta}_b/2}d\bar{\theta}\int_{-\bar{\theta}_b/2}^{\bar{\theta}_b/2}d\bar{\theta}'\langle\bar{I}_1(\bar{\theta})\bar{I}_1^*(\bar{\theta}')\rangle-W_1^2\\=&\bar{\theta}_b\bar{I}_1^2\int_{-\bar{\theta}_b/2}^{\bar{\theta}_b/2}d\vartheta|\gamma_{G_1}(\vartheta)|^2.\end{aligned} \tag{B5}$$

Here we have used the moment theorem for the complex Gaussian random variables [29] in deriving the last expression, and γ_{G_1} is known to be the complex degree of coherence of the light [29], i.e.,

$$|\gamma_{G_1}(\bar{\theta}-\bar{\theta}')|=\frac{|\langle G_1(\bar{\theta})G_1^*(\bar{\theta}')\rangle|}{\langle|G_1(\bar{\theta})|^2\rangle}=\exp\left(\frac{-\vartheta^2}{8\sigma_{\bar{\theta}}^2}\right). \tag{B6}$$

Thus, the rms fluctuation for the fundamental radiation energy is

$$\sqrt{\frac{W_1^2}{\sigma_{W_1}^2}}\approx\left(\frac{\bar{\theta}_b}{2\sqrt{\pi}\sigma_{\bar{\theta}}}\right)^{1/2}\equiv\sqrt{M_c}, \tag{B7}$$

where M_c is roughly the number of coherent modes in a bunch.

From Eq. (50), the temporal structure of the third nonlinear harmonic is approximately governed by G_1^3. We can obtain the ''intensity'' of the third nonlinear harmonic by using Eq. (B4) for $n=6$:

$$\bar{I}_3=\langle G_1^3(G_1^*)^3\rangle=\langle|G_1|^6\rangle=6\bar{I}_1^3. \tag{B8}$$

The third-harmonic energy is integrated along the pulse and is $W_3=\bar{I}_3\bar{\theta}_b$. Following the derivation for fundamental radiation, the variance of the third-harmonic energy is

$$\sigma_{W_3}^2=\int_{-\bar{\theta}_b/2}^{\bar{\theta}_b/2}d\bar{\theta}\int_{-\bar{\theta}_b/2}^{\bar{\theta}_b/2}d\bar{\theta}'\langle\bar{I}_3(\bar{\theta})\bar{I}_3^*(\bar{\theta}')\rangle-W_3^2$$

$$=\frac{W_3^2}{\bar{\theta}_b}\int_{-\bar{\theta}_b/2}^{\bar{\theta}_b/2}d\vartheta[9|\gamma_{G_1}(\vartheta)|^2+9|\gamma_{G_1}(\vartheta)|^4+|\gamma_{G_1}(\vartheta)|^6]. \tag{B9}$$

Using Eq. (B6), we obtain the rms fluctuation for the third-harmonic energy

$$\sqrt{\frac{W_3^2}{\sigma_{W_3}^2}}\approx\left[\left(9+\frac{9}{\sqrt{2}}+\frac{1}{\sqrt{3}}\right)^{-1}\frac{\bar{\theta}_b}{2\sqrt{\pi}\bar{\sigma}_\theta}\right]^{1/2}\approx\frac{\sqrt{M_c}}{4}. \tag{B10}$$

Hence, the third nonlinear harmonic signal is about four times more noisy than the fundamental in this sense.

APPENDIX C: BUNCHING PARAMETER

In FEL simulation programs such as GINGER [30], a bunching parameter is used to indicate the level of the microbunching due to the FEL interaction. For simulations that keep track of N_s independent beam slices (of length λ_r), a natural definition would be

$$b_h=|\langle e^{-ih\theta_j}\rangle|$$

$$=\left|\int\frac{d\bar{x}^2}{2\pi\bar{\sigma}_x^2}\int d\bar{p}^2\int d\bar{\eta}\int_0^{2\pi N_s}\frac{d\theta}{2\pi N_s}e^{-ih\theta}f(\bar{z},\theta,\bar{\eta},\bar{x},\bar{p})\right|$$

$$<1. \tag{C1}$$

This is indeed the definition for the third-harmonic bunching in GINGER [31], but the fundamental bunching parameter is defined with respect to the fundamental field phase ψ, i.e., $b_1=|\langle e^{-i(\theta+\psi)}\rangle|$. From Sec. IV and V, we know the dominant component in the distribution function that drives the third-harmonic bunching is

$$e^{3i\theta}\int_0^{\bar{z}}d\bar{s}_1e^{i\phi(\bar{s}_1-\bar{z})}\tilde{a}_1(\bar{\theta},\bar{x}_1^{(0)},\bar{s}_1)\frac{\partial}{\partial\bar{\eta}}\int_0^{\bar{s}_1}d\bar{s}_2e^{i\phi(\bar{s}_2-\bar{z})}$$

$$\times\tilde{a}_1(\bar{\theta},\bar{x}_2^{(0)},\bar{s}_2)\frac{\partial}{\partial\bar{\eta}}\int_0^{\bar{s}_2}d\bar{s}_3e^{i\phi(\bar{s}_3-\bar{z})}(\bar{\theta},\bar{x}_3^{(0)},\bar{s}_3)\frac{\partial f_0}{\partial\bar{\eta}}. \tag{C2}$$

For CA, $\tilde{a}_1$ is constant in $\bar{\theta}$; for SASE, $\tilde{a}_1$ is approximated by Eq. (49). In both cases, we can carry out the integrals in $\bar{x},\bar{p},\bar{\eta}$ as before and obtain

$$b_3=e^{3\,\mathrm{Im}(\mu_0)\bar{z}}\bar{A}_0^3\left|\int_{-\infty}^0d\tau_1\int_{-\infty}^0d\tau_2\int_{-\infty}^0d\tau_3\right.$$

$$\times\frac{3\tau_1(3\tau_1+2\tau_2)(3\tau_1+2\tau_2+\tau_3)}{4w_1^2U}$$

$$\left.\times\exp\left[-\frac{\bar{\sigma}_\eta^2}{2}(3\tau_1+2\tau_2+\tau_3)^2-i\mu_0(3\tau_1+2\tau_2+\tau_3)\right]\right|$$

$$\times\begin{cases}1 & \text{CA},\\ \langle|G_1^3|\rangle & \text{SASE},\end{cases} \tag{C3}$$

where U is defined in Eq. (46), and G_1 is the longitudinal random phasor sum. Using the relation for the fundamental radiation power and Eq. (B4) for $n=3$, we can write the third-harmonic bunching as

$$b_3=8w_{1r}^{3/2}\left(\frac{P_1}{\rho P_{\mathrm{beam}}}\right)^{3/2}\left|\int_{-\infty}^0d\tau_1\int_{-\infty}^0d\tau_2\int_{-\infty}^0d\tau_3\right.$$

$$\times\frac{3\tau_1(3\tau_1+2\tau_2)(3\tau_1+2\tau_2+\tau_3)}{4w_1^2U}$$

$$\left.\times\exp\left[-\frac{\bar{\sigma}_\eta^2}{2}(3\tau_1+2\tau_2+\tau_3)^2-i\mu_0(3\tau_1+2\tau_2+\tau_3)\right]\right|$$

$$\times\begin{cases}1 & \text{CA},\\ 1.3 & \text{SASE}.\end{cases} \tag{C4}$$

[1] W. B. Colson, IEEE J. Quantum Electron. **QE-17**, 1417 (1981).

[2] L. H. Yu, Phys. Rev. A **44**, 5178 (1991).

[3] R. Bonifacio, L. De Salvo, and P. Pierini, Nucl. Instrum. Methods Phys. Res. A **293**, 627 (1990).

[4] H. P. Freund, S. G. Biedron, and S. V. Milton, IEEE J. Quantum Electron. **QE-36**, 275 (2000); Nucl. Instrum. Methods Phys. Res. A **445**, 53 (2000).

[5] M. Xie, Nucl. Instrum. Methods Phys. Res. A **445**, 59 (2000); **445**, 67 (2000).

[6] M. J. Schmitt and C. J. Elliott, Phys. Rev. A **34**, 4843 (1986); **41**, 3853 (1990); Nucl. Instrum. Methods Phys. Res. A **296**, 394 (1990).

[7] Z. Huang and K.-J. Kim, in *Proceedings of the 22nd International Free Electron Laser Conference, Durham, 2000* (Elsevier, Amsterdam, in press).

[8] Y. L. Klimontovich, Zh. Eksp. Teor. Fiz. **33**, 982 (1957) [Sov. Phys. JETP **6**, 753 (1958)]; see also Ref. [11].

[9] E. T. Scharlemann, J. Appl. Phys. **58**, 2154 (1985).

[10] E. L. Saldin, E. A. Schneidmiller, and M. V. Yurkov, in *Proceedings of the 22nd International Free Electron Laser Conference, Durham, 2000* (Ref. [7], and Ref. 20 therein.

[11] S. Ichimaru, *Basic Principles of Plasma Physics* (W. A. Benjamin, Inc., London, 1973).

[12] R. Bonifacio, C. Pellegrini, and L. M. Narducci, Opt. Commun. **50**, 373 (1984).

[13] K.-J. Kim, Phys. Rev. Lett. **57**, 1871 (1986).

[14] L.-H. Yu, S. Krinsky, and R. L. Gluckstern, Phys. Rev. Lett. **64**, 3011 (1990).

[15] J. B. Murphy, C. Pellegrini, and R. Bonifacio, Opt. Commun. **53**, 197 (1985).

[16] 1D analysis of SASE has been given by K.-J. Kim, Nucl. Instrum. Methods Phys. Res. A **250**, 396 (1986); and by J.-M.

Wang and L.-H. Yu, *ibid.* **250**, 484 (1986).
[17] R. Bonifacio, R. Corsini, and P. Pierini, Phys. Rev. A **45**, 4091 (1992).
[18] S. V. Milton, E. Gluskin, N. D. Arnold, S. Berg, W. Berg, Y.-C. Chae, E. A. Crosbie, R. J. Dejus, P. D. Hartog, H. Friedsam, H. N. Galayda, A. Grelick, J. Jones, Y. Kang, S. Kim, J. W. Lewellen, A. H. Lumpkin, J. R. Maines, G. M. Markovich, E. R. Moog, A. Nassiri, E. Trakhtenberg, I. Vasserman, N. Vinokurov, D. R. Walters, J. Wang, and B. Yang, Nucl. Instrum. Methods Phys. Res. A **407**, 210 (1998).
[19] K.-J. Kim and M. Xie, Nucl. Instrum. Methods Phys. Res. A **331**, 359 (1993).
[20] Linac Coherent Light Source Design Study Report, SLAC-R-521, 1998.
[21] S. V. Milton and S. G. Biedron (private communication).
[22] C. Pellegrini (private communication).
[23] L.-H. Yu, M. Babzien, I. Ben-Zvi, L. F. DiMauro, A. Doyuran, W. Graves, E. Johnson, S. Krinsky, R. Malone, I. Pogorelsky, J. Skaritka, G. Rakowsky, L. Solomon, X. J. Wang, M. Woodle, V. Yakimenko, S. G. Biedron, J. N. Galayda, E. Gluskin, J. Jagger, V. Sajaev, and I. Vasserman, Nucl. Instrum. Methods Phys. Res. A **445**, 301 (2000).
[24] S. G. Biedron (private communication).
[25] N. G. Van Kampen, Physica (Utrecht) **21**, 949 (1955); K. M. Case, Ann. Phys. (N.Y.) **7**, 349 (1959).
[26] M. Xie, presented at the American Physical Society April Meeting, Long Beach, 2000.
[27] K.-J. Kim, in *Towards X-ray Free Electron Lasers*, edited by R. Bonifacio and W. A. Barletta (AIP, New York, 1997).
[28] E. L. Saldin, E. A. Schneidmiller, and M. V. Yurkov, Opt. Commun. **148**, 383 (1998).
[29] J. W. Goodman, *Statistical Optics* (Wiley, New York, 1985).
[30] W. M. Fawley, *An Informal Manual for* GINGER *and its Post-processor XPLOTGIN* (CBP Tech Note-104, Lawrence Berkeley Laboratory, 1995).
[31] W. M. Fawley (private communication).